AN APPROACH TO SIZING A DUAL-USE BALLUTE SYSTEM FOR AEROCAPTURE, DESCENT, AND LANDING

Kristin L. Gates Medlock[(1)] and James M. Longuski[(2)],
[(1)] *Doctoral Candidate, Purdue University, Aeronautics & Astronautics, West Lafayette, IN 47907-2023, USA*
Email: gatesk@purdue.edu
[(2)] *Professor, Purdue University, Aeronautics & Astronautics, West Lafayette, IN 47907-2023, USA*
Email: longuski@ecn.purdue.edu

ABSTRACT

A dual-use ballute system for aerocapture and descent at the atmosphere-bearing planets and at Titan may provide significant performance benefits. The ballute's large area-to-mass ratio allows the vehicle to stay high in the atmosphere where the heating rate is low. Once the desired velocity change is achieved, the ballute is released allowing the orbiter to continue on its capture orbit, while the ballute/lander (or ballute/probe) descends to the denser regions of the atmosphere.

Sizing of the dual-use ballute is driven by several factors including the target orbit, ballute material limits, and the planetary atmosphere. Using Vinh's analytic theory for aerocapture and ballistic fly-through trajectories, we present an expression for the maximum heating rate as a function of velocity, atmospheric density, scale height, nose radius, and ballistic coefficient. Once we specify a capture trajectory, the maximum heating-rate expression is used to determine the approximate size (i.e. the ballistic coefficient) of the ballute. We test the accuracy of our sizing algorithm for aerocapture and descent trajectories at Mars, Titan, Neptune, and Earth.

NOMENCLATURE

A	=	aerodynamic reference area, m^2
C_B	=	ballistic coefficient, kg/m^2
C_D	=	aerodynamic drag coefficient
g	=	gravitational acceleration, m/s^2
h_e	=	reference (entry) altitude, m/s^2
m	=	mass, kg
Q	=	heating rate, W/cm^2
R	=	radius of the atmosphere, km
R_n	=	nose radius, m
r	=	radial distance, km
t	=	time, s
v	=	speed, km/s
v_c	=	circular speed, km/s
v_e	=	entry speed, km/s
x	=	non-dimensional speed variable
Z	=	non-dimensional altitude variable
α	=	non-dimensional speed ratio parameter
β	=	inverse scale height, km^{-1}
ϕ	=	non-dimensional flight path angle variable
γ	=	flight path angle, deg
ρ	=	atmospheric density, kg/m^3
ρ_e	=	reference atmospheric density, kg/m^3

1. INTRODUCTION

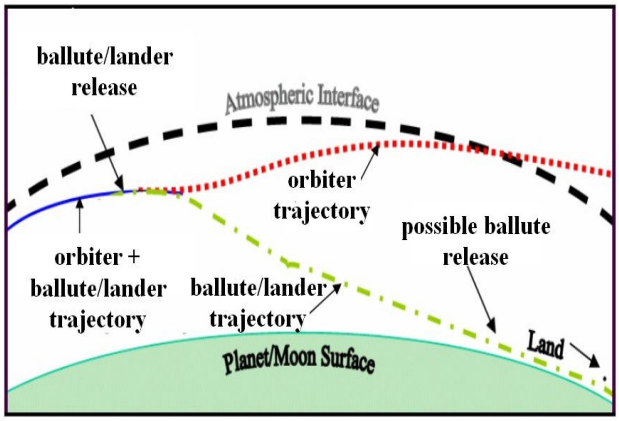

Fig. 1. Dual-Use Ballute Schematic

Because of performance advantages and mass savings potential, a significant amount of research has been carried out to investigate the feasibility of different ballute systems and missions. A systems level study of ballutes for aerocapture at several planetary bodies has been conducted by McRonald [1,2] and an extensive review of ballute technology is provided by Hall [3]. K. Miller et al. [4] characterize and refine the use of ballutes for future aerocapture missions and the Inspace Propulsion group at Marshall Spaceflight Center has published a paper on inflatable decelerator investments [5]. Recent studies by Lyons and McRonald [6] and Medlock et al. [7] present preliminary studies on the feasibility of using dual-use ballute systems at Mars, Titan, and Neptune.

2. VINH'S SECOND-ORDER THEORY FOR BALLISTIC AEROCAPTURE TRAJECTORIES

We make use of Vinh's second-order theory for ballistic aerocapture trajectories [8] to analyze dual-use ballute trajectories. To size the ballute, we derive a transcendental expression for the maximum heating rate as a function of ballistic coefficient and entry trajectory.

Dual-use ballute studies have shown that the ballute/lander is typically released shortly after peak conditions (i.e. when heating, deceleration, and dynamic pressure have already reached their maximums). Because the descent trajectory does not produce heating rates larger than those prior to release, we do not examine the trajectory after release. Instead, we employ Vinh's capture theory for (a worst-case) analysis of the entire dual-use ballute system. Next we present a brief review of the analytical capture theory, details of which can be found in Refs.8 and 9.

Vinh et al. [8,10] give the following planar equations of motion for a non-rotating planet:

$$\frac{dr}{dt} = v\sin\gamma \tag{1}$$

$$\frac{dv}{dt} = \frac{-D}{m} - g\sin\gamma \tag{2}$$

$$\frac{d\gamma}{dt} = -\frac{1}{v}\left(g - \frac{v^2}{r}\right)\cos\gamma \tag{3}$$

The atmosphere is assumed the be locally exponential and is given by

$$d\rho = -\beta(r)\rho dr \tag{4}$$

The assumptions given in Eqs. (5)–(6) are applied to Eqs. (1)–(3),

$$\begin{aligned} g(r) &\approx g(R) \\ \frac{v^2}{r} &\approx \frac{v^2}{R} \end{aligned} \tag{5}$$

$$-g\sin\gamma = 0 \tag{6}$$

resulting in the simplified equations of motion presented in Eqs. (7)–(9).

$$\frac{dr}{dt} = v\sin\gamma \tag{7}$$

$$\frac{dv}{dt} = \frac{-\rho S C_d v^2}{2m} \tag{8}$$

$$\frac{d\gamma}{dt} = -\frac{1}{v}\left(g - \frac{v^2}{R}\right)\cos\gamma \tag{9}$$

Vinh uses the non-dimensional variables given in Eqs. (10)–(12), representing altitude, flight path angle, and speed, respectively.

$$Z = \rho S C_D m^{-1}\left(R/\beta\right)^{1/2} \tag{10}$$

$$\phi = -\left(\beta R\right)^{1/2}\sin\gamma \tag{11}$$

$$x = \log\left(v_e^2/v^2\right) \tag{12}$$

An additional non-dimensional variable, α, specifies the type of entry orbit (i.e. hyperbolic: $\alpha < 0.5$, parabolic: $\alpha = 0.5$, elliptic: $\alpha > 0.5$).

$$\alpha = gR/v_e^2 = v_c^2/v_e^2 \tag{13}$$

Dividing the time derivatives of Eqs. (10) and (11) by the time derivative of Eq. (12) and applying the small angle approximation in Eq. (14),

$$\left(\cos\gamma \approx 1\right) \tag{14}$$

provide equations of motion

$$\frac{dZ}{dx} = \phi \tag{15}$$

$$\frac{d\phi}{dx} = \left(\alpha e^x - 1\right)Z^{-1} \tag{16}$$

with initial conditions

$$\begin{aligned} &x = 0, \\ &Z(0) = \varepsilon = \rho_e S C_D m^{-1}\left(R/\beta\right)^{1/2}, \\ &\phi(0) = c = -\left(\beta R\right)^{1/2}\sin\gamma_e \end{aligned} \tag{17}$$

To facilitate integration by use of Poincare's method of artificially inserting a small parameter, a final change of variables is made,

$$y = Z/\varepsilon \tag{18}$$

$$\tau = x/\varepsilon \tag{19}$$

$$d(\ )/d\tau = (\ )' \tag{20}$$

to get Eqs. (21) and (22),

$$y' = \phi \tag{21}$$

$$\phi' = \left(\alpha e^{\varepsilon\tau} - 1\right)/y \tag{22}$$

with initial conditions,

$$\tau = 0,\ \ y(0) = 1,\ \ \ \phi(0) = c \tag{23}$$

Using drag parameter ε, we look for solutions of the form:

$$\begin{aligned} y &= y_0 + \varepsilon y_1 + \varepsilon^2 y_2 + \ldots \\ \phi &= \phi_0 + \varepsilon\phi_1 + \varepsilon^2\phi_2 + \ldots \end{aligned} \tag{24}$$

with initial conditions

$$\begin{aligned} &y_0(0) = 1, \quad y_1(0) = y_2(0) = \ldots = 0 \\ &\phi_0(0) = c, \quad \phi_1(0) = \phi_2(0) = \ldots = 0 \end{aligned} \tag{25}$$

Substituting Eq. (24) into Eqs. (15) and (16) and equating like terms of ε, gives the following system of equations:

$$y_0' = \phi_0 \tag{26}$$

$$\phi_0' = -(1-\alpha)\, y_0^{-1} \tag{27}$$

$$y_1' = \phi_1 \tag{28}$$

$$\phi_1' = (1-\alpha)\, y_1 y_0^{-2} + \alpha\tau y_0^{-1} \tag{29}$$

$$y_2' = \phi_2 \tag{30}$$

$$\begin{aligned} \phi_1' = {} & (1-\alpha)\, y_2 y_0^{-2} - \alpha\tau y_1 y_0^{-2} \\ & + \frac{1}{2}\alpha\tau^2 y_0^{-1} - (1-\alpha)\, y_1^2 y_0^{-3} \end{aligned} \tag{31}$$

After some labor, solutions for the 0th, 1st, and 2nd order systems are obtained. (See references 1 and 2 for details).

1.1. Zero-Order Analytic Solutions

The independent variable ϕ_0 (representing the zero-order flight path angle) monotonically increases from its initial value c. The zero-order solution for the altitude variable, y, is

$$y_0 = \exp\left[\left(c^2 - \phi_0^2\right)/\delta\right] \tag{32}$$

where

$$\delta = 2(1-\alpha) \tag{33}$$

represents the entry speed. The analytical expression for τ, representing the speed variable is

$$\tau = \sqrt{\frac{\pi}{\delta}}\exp\left(\frac{c^2}{\delta}\right)\left[erf\left(\frac{c}{\sqrt{\delta}}\right) - erf\left(\frac{\phi_0}{\sqrt{\delta}}\right)\right] \tag{34}$$

where the error function is defined as

$$erf(x) = 2\pi^{-1/2}\int_0^x e^{-t^2}dt \tag{35}$$

1.2. First-Order Analytic Solutions

The first-order solution coefficients for y and ϕ are

$$y_1 = 2\alpha\delta^{-2}\phi_0 + 2\alpha\delta^{-2}k\left(y_0 - \phi_0\tau\right) \tag{36}$$

$$\phi_1 = \alpha\delta^{-1}\left(k\tau - 1\right)y_0^{-1} + \alpha\delta^{-1}\left(y_0 - \phi_0\tau\right) \tag{37}$$

where,

$$k = (1-\alpha)\tau - c \tag{38}$$

1.3. Second-Order Analytic Solutions

The second-order solution coefficients for y and ϕ are

$$\begin{aligned} y_2 &= 2\alpha\delta^{-3}\left(y_0-\phi_0\tau\right)\left[\left(1+\alpha\right)+\left(1-\alpha\right)\tau^2\right] \\ &+\alpha\delta^{-3}\phi_0\tau\left[\alpha+\left(\delta/6\right)\left(\alpha+2\right)\tau^2\right] \\ &-\alpha\delta^{-3}\left(\alpha+2\right)y_0^3-\alpha^2\delta^{-3}\left(k\tau-1\right)^2 y_0^{-1} \\ &+\alpha\delta^{-2}ky_1-6\alpha\delta^{-4}\left(\alpha+2\right)\phi_0\left[K\left(\phi_0\right)-K\left(c\right)\right] \end{aligned} \tag{39}$$

$$\begin{aligned} \phi_2 &= 2\alpha\delta^{-2}\left(y_0-\phi_0\tau\right)\tau \\ &+\alpha\delta^{-3}\phi_0\left[\alpha+\left(1+\alpha\right)\left(\alpha+2\right)\tau^2\right] \\ &+\left(\delta/6\right)\delta^{-2}\tau y_0^{-1}\left[3\left(\alpha+2\right)+\left(1-\alpha\right)\left(4-\alpha\right)\tau^2\right] \\ &+\alpha^2\delta^{-3}\left(k\tau-1\right)^2\phi_0 y_0^{-2}+\left(\alpha/2\right)\delta^{-1}y_1+\alpha\delta^{-2}k\phi_1 \\ &-2\alpha^2\delta^{-3}\left(k\tau-1\right)y_0^{-1}\left[k+\left(1-\alpha\right)\tau\right] \\ &+3\alpha\delta^{-3}\left(\alpha+2\right)y_0^{-1}\left[K\left(\phi_0\right)-K\left(c\right)\right] \end{aligned} \tag{40}$$

where,

$$K\left(\phi_0\right)=\left(\delta\pi/12\right)^{1/2}\exp\left(3c^2/\delta\right)erf\left[\left(3/\delta\right)^{1/2}\phi_0\right] \tag{41}$$

3. THE HEATING CONSTRAINT

Stagnation-point heating rate during atmospheric flight is calculated by,

$$Q_{stag}=\frac{C\rho^{Nstag}v^{Mstag}}{\sqrt{R_n}} \tag{42}$$

(similar to the Sutton-Graves convective heating equation [11]). In Eq. (42), N_{stag} and M_{stag} are the density and velocity coefficients (typical values of N_{stag} = 0.5 and M_{stag} = 3.0 are used for this study), and C is the stagnation point heating coefficient. The stagnation-point heating coefficient (C) varies according to the planet. We use 9.748 x 10^{-5}, 9.80 x 10^{-5}, 9.00 x $10^{-5}$and 3.54 x 10^{-5} $kg^{0.5}$/m for Earth, Mars, Titan and Neptune, respectively. The R_n of the ballute/lander is calculated assuming a spherical ballute.

Eq. (42) can be written as

$$Q_{stag}=C_H\left(\frac{\rho}{\rho_e}\right)^{1/2}\left(\frac{v}{v_e}\right)^3 \tag{43}$$

where

$$C_H=C\left(\frac{\rho_e}{R_n}\right)^{1/2}v_e^3 \tag{44}$$

From Eqs. (10), (12), (18), and (19), we see that,

$$\frac{\rho}{\rho_e}=y \tag{45}$$

and

$$\frac{v}{v_e}=e^{-\tau\varepsilon/2} \tag{46}$$

Substituting Eqs. (45) and (46) into Eq. (43) gives an expression for stagnation point heating rate as a function of the nondimensional variables y, τ, and ε (representing altitude, speed, and ballistic coefficient, respectively):

$$Q_{stag}=C_H y^{1/2}e^{-3\tau\varepsilon/2} \tag{47}$$

To evaluate conditions at the point of maximum instantaneous heating rate, we differentiate Eq. (47) with respect the speed variable τ.

$$\frac{d\left(Q_{stag}\right)}{d\tau}=0=\frac{C_H}{2}\left[y'y^{-1/2}e^{-3\tau\varepsilon/2}-3\varepsilon y^{1/2}e^{-3\tau\varepsilon/2}\right] \tag{48}$$

Recalling that $y'=\phi$, Eq. (48) simplifies to

$$\phi=3\varepsilon y \tag{49}$$

Eq. (49) provides the key that relates the speed variable, flight path angle variable, and ballistic coefficient at the point of peak heating. Substituting this equation into the nondimensional heating rate expression, in Eq. (47), gives an equation for maximum heating rate as a function of ϕ_0:

$$Q_{stag,\max}=C_H\left(\frac{\phi}{3\varepsilon}\right)^{1/2}e^{-3\tau\varepsilon/2} \tag{50}$$

In order to solve for ϕ in Eq. (50), we derive an expression for ϕ_0, at the point of peak heating. Using Eq. (49) and the zero-order solution for y given in Eq.

(32), we obtain an implicit (or transcendental) expression for ϕ_0:

$$\phi_0 = 3\varepsilon y_0 = 3\varepsilon y_0 \, e^{c^2/\delta} \, e^{-\phi_0^2/\delta} \tag{51}$$

Using the approximation,

$$e^{-\phi_0^2/\delta} \approx 1 - \frac{\phi_0^2}{\delta} \tag{52}$$

we obtain an explicit expression for ϕ_0:

$$\phi_0 = \frac{-\delta}{6\varepsilon}\left[e^{-c^2/\delta} - \sqrt{e^{-2c^2/\delta} - \frac{36\varepsilon}{\delta}} \right] \tag{53}$$

We can now use Eq. (53) with Eqs. (32)–(41) and Eq. (24) to obtain 0th, 1st, and 2nd order solutions for y and ϕ at the point of peak heating in terms of the ballistic coefficient (represented by ε) and the entry conditions (α, representing entry speed, and c, representing entry flight path angle). Depending on the desired accuracy, any order of the ϕ solution can be used in Eq. (49) to determine the appropriate ballute size (ε value) for a given maximum heating rate limit.

4. NUMERICAL RESULTS

In this section we consider the problem of sizing the ballute for missions at Earth, Mars, Titan , and Neptune [4,12-16] with a wide range of entry conditions and allowable heating rates. Although the analysis depends on the ballistic coefficient, we provide (in Table 1) some specific values for a typical dual-use ballute system in which the ballute area may range from 500-3000 m^2.

Table 1 Vehicle Parameters for Dual-Use Ballute Simulations at Earth, Mars, Titan and Neptune.

Parameter	Orbiter	Ballute/Lander
m	400 kg	100 kg
C_D	1.37	1.37
A	2 m^2	500–3000 m^2 *
R_n	0.8 m	15.5 m
C_B	$m/(C_D A)$	0.730–0.122 kg/m^2

* Representative of the ballistic coefficient range used.

The range of entry speeds examined at Earth, Mars, Titan, and Neptune are adapted from previous studies [6, 12–15] and are displayed in Table 2.

Table 2 Entry Conditions and Atmospheric Constants at Earth, Mars, Titan, and Neptune.

Condition	Earth	Mars	Titan	Neptune
βR	900	350	56	441
reference density, kg/m^2	2.22e-8	4.73e-10	7.52e-10	1.48E-14
Entry/Exit Altitude, km	120	150	1025	1500
Inertial Entry Speeds, km/s	12.9	5.75–11	6.5–10	23.6

For this particular study, we are concerned only with the segment of the trajectory prior to release of the ballute/lander (this is the time during which the maximum heating rate occurs).

We choose an entry flight path angle that targets a circular orbit at exit (assuming the ballute/lander is not released). Because the target apoapsis altitude of the orbiter is higher than that of the chosen circular exit orbit, the ballute/lander will be released inside the atmosphere and continue its descent. This method allows the vehicle to dive deep enough to accommodate navigation and atmospheric uncertainties while maintaining a high enough trajectory to keep the heating rates low.

The altitude variable is represented by the dimensionless density y, normalized with respect to the density at the entry altitude (ρ_e). The variation of the linear altitude h is provided through y:

$$\beta\left(h - h_e\right) = \beta\Delta h = -\log y \tag{54}$$

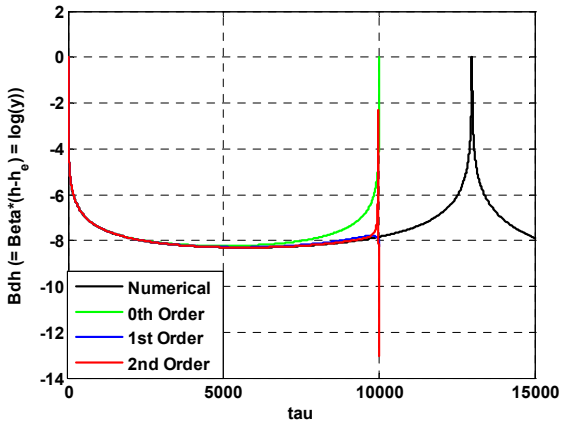

Fig. 1. Variation of Linear Altitude vs. Representative Speed Variable (τ).

In our first case we consider a Martian entry with an entry velocity of 5.75 km/s. The analytic solutions in Fig. 1 show excellent agreement (with the numerical integration of Eqs. (15) and (16)) through the critical segment of the trajectory, but underestimates the total velocity lost prior to exiting the atmosphere . This discrepancy is partially attributed to the small angle approximation made during derivation of the analytic solutions, and is expected to increase with the steepness of the entry angles.

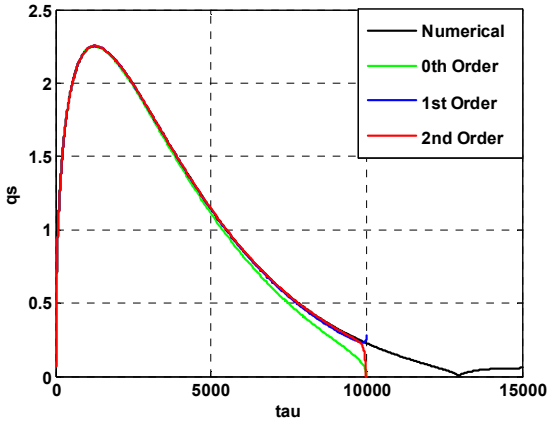

Fig. 2. Stagnation Point Heating Rate vs. Representative Speed Variable, τ, at Mars with v_e = 5.75 km/s.

Fig.2 displays the heating rates continuously calculated using the 0th, 1st, and 2nd order analytic solutions along with the heating profile obtained through numerical integration. Again, the analytic solutions show excellent agreement throughout the crucial portion of the trajectory, just slightly underestimating the peak heating rate.

Next, we evaluate the accuracy of Eqs. (50) and (53) in predicting the maximum heating rate. Tables 3–7 provide errors for the predicted heating rate for varying entry speeds at both Mars and Titan. As entry speed, at either planet, increases (resulting in a steeper entry) the percent error of the analytic heating expression increases due in part to the truncation error in Eq. (52). (Here we note that a more accurate prediction may be possible by solving the transcendental Eq. (51) for ϕ_0, where the explicit solution Eq. (53) provides a useful first guess.) We show only the 0th order heating rate errors in Tables 3–7 because the higher order errors are nearly indistinguishable from the 0th order. For example, in Table 5 for the case C_B = 0.12 kg/m^2, the heating rate errors for 0th, 1st, and 2ne order ar 11.83%, 11.80%, and 11.80%, respectively. (Again, a better prediction may be obtained by solving the transcendental expression in Eq. (52).

Table 3 Zero-Order Heating Rate Error for Mars, v_e= 5.75 km/s, α= 0.37, m = 500 kg, C_D= 1.37

C_B [kg/m^2]	A [m^2]	R_n [m]	ε *10^{-4}	γ_e [deg]	Heating Rate Error %
0.73	500	12.6	1.23	-9.50	2.60%
0.49	750	15.5	1.84	-9.23	2.59%
0.36	1000	17.8	2.46	-9.04	2.60%

Table 4 Zero-Order Heating Rate Error for Mars, v_e= 7.00 km/s, α= 0.25, m = 500 kg, C_D= 1.37

C_B [kg/m^2]	A [m^2]	R_n [m]	ε *10^{-4}	γ_e [deg]	Heating Rate Error %
0.49	750	15.5	1.84	-10.40	4.24%
0.36	1000	17.8	2.46	-10.20	4.28%
0.24	1500	21.9	3.69	-9.91	4.28%

Table 5 Zero-Order Heating Rate Error for Mars, v_e= 11.0 km/s, α= 0.10, m = 500 kg, C_D= 1.37

C_B [kg/m^2]	A [m^2]	R_n [m]	ε *10^{-4}	γ_e [deg]	Heating Rate Error %
0.49	750	15.5	1.84	-11.88	11.62%
0.24	1500	21.9	3.69	-11.36	11.64%
0.12	3000	30.9	7.37	-10.83	11.83%

Table 6 Zero-Order Heating Rate Error for Titan, v_e= 6.75 km/s, α= 0.06, m = 500 kg, C_D= 1.37

C_B [kg/m^2]	A [m^2]	R_n [m]	ε *10^{-4}	γ_e [deg]	Heating Rate Error %
0.49	750	15.5	7.43	-29.28	16.91%
0.24	1500	21.9	14.9	-27.70	16.97%

Table 7 Zero-Order Heating Rate Error for Titan, v_e= 10.0 km/s, α= 0.02, m = 500 kg, C_D= 1.37

C_B [kg/m^2]	A [m^2]	R_n [m]	ε *10^{-4}	γ_e [deg]	Heating Rate Error %
0.49	750	15.5	7.43	-30.66	25.88%
0.36	1000	17.8	9.91	-30.00	25.85%
0.24	1500	21.9	14.9	-29.05	25.77%
0.12	3000	30.9	29.7	-27.39	25.77%

Fig. 3 plots the ballistic coefficient (calculated using the area of the ballute) plotted against the maximum stagnation point heating rate of the ballute (calculated

using an R_n that varies with the ballute size). Similarly, Fig. 4 provides values for the orbiter (R_n = 0.8 m^2). Assuming a maximum heating limit of 5 W/cm^2 on the ballute, Fig. 3 indicates that any of the ballute sizes shown will work (the most cost effective, of course, being the smallest). However, applying the same heating limit to the orbiter, Fig.4 shows that only the lowest of the entry velocity cases at Mars and Titan stay within the limit (for the sizes plotted), suggesting that a thermal protection system (TPS) may be required on the orbiter. It is interesting to note that the cases for Titan with v_e = 6.50 km/s and Mars with v_e = 5.75 km/s follow nearly the same contour.

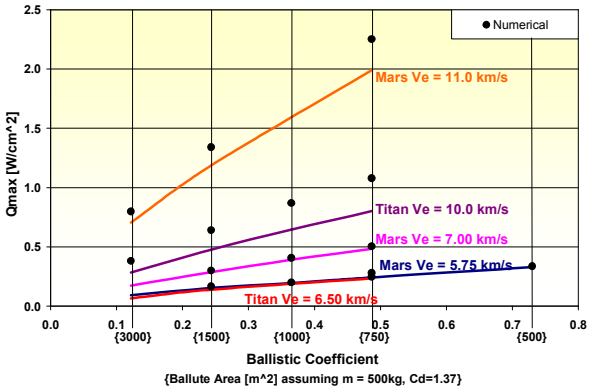

Fig. 3. Maximum Stagnation Point Heating Rate (on Ballute) vs. Ballistic Coefficient

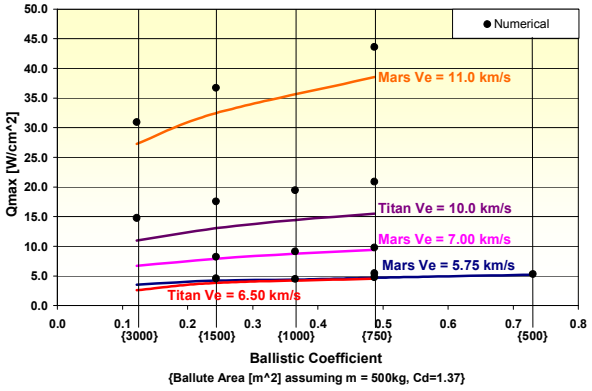

Fig. 4. Maximum Stagnation Point Heating Rate (on Orbiter) vs. Ballistic Coefficient

Numerical and analytical results for missions to Neptune and return missions to the Earth (e.g. from the Moon) indicate heating error trends similar to those at Mars and Titan. For instance, a case at Neptune (v_e = 23.6 km/s) with an entry angle of -10° has less than 1% error, whereas a case with the same entry velocity and an entry angle of -11° has a 15% error.

5. CONCLUSIONS

It appears that the zero-order theory gives adequate results to predict the maximum heating rate, when compared to the first- and second-order results. Using the analytic solution in the zero-order theory, we found an underestimation ranging from -0.002 W/cm^2 (best Mars case) to -0.120 W/cm^2 (worst Titan case) for heating on the ballute and from -0.140 W/cm^2 to -4.41 W/cm^2 for heating on the orbiter (with A = 2 m^2). The less hyperbolic the entry speed (and likewise, the shallower the entry angle for a specified target orbit), the more accurate the explicit theory is. It is expected that the implicit expression will provide more accurate results.

For practical ballute sizes, dual-use ballute concept appears feasible at Mars, Titan, and Earth. As shown in earlier work, dual-use ballute aerocapture and descent at Neptune is highly challenging in that a very large ballute for a given mass, may be required.

Overall, the dual-use ballute concept promises tremendous potential for exploration of atmosphere bearing bodies in the Solar System.

6. ACKNOWLEDGEMENTS

The work described in this paper was funded by NASA's Graduate Student Research Program (GSRP) awarded by Marshall Space Flight Center in Huntsville, Ala. We would particularly like to thank Bonnie James at MSFC for her support. Also, we would like to thank Mohammad Ayoubi (a doctoral candidate at Purdue University) for his assistance.

7. REFERENCES

1. McRonald, A. D., "A Light-Weight Inflatable Hypersonic Drag Device for Planetary Entry," Association Aeronautique de France Conf. at Arcachon France, March 16-18, 1999.

2. McRonald, A. D., "A Light-Weight Hypersonic Inflatable Drag Device for a Neptune Orbiter," AAS/AIAA Space Flight Mechanics Meeting, Clearwater, FL, AAS Paper 00-170, Jan. 23-26, 2000.

3. Hall, J. L., "A Review of Ballute Technology For Planetary Aerocapture," 4th IAA Conference on Low Cost Planetary Missions, Laurel, MD, May 2-5, 2000.

4. Miller, K. L., Gulick, D., Lewis, J., Trochman, B., Stein, J., Lyons, D. T., and Wilmoth, R., "Trailing

Ballute Aerocapture: Concept and Feasibility Assessment," 39th AIAA/ASME/ASEE Joint Propulsion Conference and Exhibit, Huntsville, AL, AIAA Paper 2003-4655, July 20-23, 2003.

5. Richardson, E. H., Munk, M. M., James, B. F., Moon, S. A., "Review of NASA In-Space Propulsion Technology Program Inflatable Decelerator Investments," 18th AIAA Aerodynamic Decelerator Systems Technology Conference and Seminar, Munich, Germany, AIAA Paper 2005-1603, May 23-26, 2005, pp.1-6.

6. Lyons, D. T., and McRonald, A. D., "Entry, Descent and Landing using Ballutes," Presentation at 2nd International Planetary Probe Workshop, NASA Ames Research Center, Moffet Field, CA, Aug. 2004.

7. Medlock, K. Gates, Longuski, J. M., and Lyons, D. T., "A Dual-Use Ballute for Entry and Descent During Planetary Missions," 3rd International Planetary Probe Workshop, Attica, Greece, June 27-July 1, 2005.

8. Vinh, N. X., Johannesen, J. R., Longuski, J. M., and Hanson, J. M., "Second-Order Analytic Solutions for Aerocapture and Ballistic Fly-Through Trajectories," The Journal of the Astronautical Sciences, Vol. 32, No. 4, Oct.-Dec. 1984.

9. Medlock, K. L. Gates, Ayoubi, M. A., Longuski, J. M., and Lyons, D. T., "Analytic Solutions for Aerocapture, Descent, and Landing Trajectories for Dual-Use Ballute Systems," To be presented at the AIAA/AAS Astrodynamics Conference, Keystone, Colorado, American Institute of Aeronautics and Astronautics, AIAA Paper 2006-6026, Aug. 2006.

10. Vinh, N.X., Busemann, A., Culp, R. D., "Hypersonic and Planetary Entry Flight Mechanics," The University of Michigan Press, Ann Arbor, MI, 1980.

11. Sutton, K. and Graves, R. A., Jr., "A General Stagnation Point Convective Heating Equation for Arbitrary Gas Mixtures," NASA TR R-376, NASA Langley Research Center, Hampton, VA, Nov. 1971.

12. Lyons, D. T. and Johnson, W. R., "Ballute Aerocapture Trajectories at Neptune," AIAA Atmospheric Flight Mechanics Conference and Exhibit, Providence, RI, AIAA Paper 2004-5181, Aug. 16-19, 2004.

13. Lyons, D. T. and Johnson, W. R., "Ballute Aerocapture Trajectories at Titan," *Advances in the Astronautical Sciences*, Vol. 116, Suppl. pp. 1-20, 2004.

14. Hall, J. L. and Le, A. K., "Aerocapture Trajectories for Spacecraft with Large, Towed Ballutes," 11th Annual AAS/AIAA Space Flight Mechanics Meeting, Santa Barbara, CA, AAS 01-235, Feb. 11-15, 2001.

15. Westhelle, C. H. and Masciarelli, J. P., "Assessment of Aerocapture Flight at Titan Using a Drag-only Device," 2003 AIAA Atmospheric Flight Mechanics Conference and Exhibit, Austin, TX, AIAA Paper 2003-5389, Aug. 11-14, 2003.

16. Vaughan, D., Miller, H. C., Griffin, B., James, B. F., Munk, M. M., "A Comparative Study of Aerocapture Missions with a Mars Destination," 41st AIAA/ASME/SAE/ASEE Joint Propulsion Conference & Exhibit, Tucson, AZ, AIAA Paper 2005-4110, July 10-13, 2005, pp. 1-16.